INTERNATIONAL JOURNAL FOR NUMERICAL METHODS IN FLUIDS, VOL. 25, 51–62 (1997)

DNS OF 2D TURBULENT FLOW AROUND A SQUARE CYLINDER

JAN G. WISSINK*

Department of Mathematics, University of Groningen, PO Box 800, NL-9700 AV Groningen, The Netherlands

SUMMARY

Two-dimensional 'turbulent' flow around a rectangular cylinder has been simulated at Re = 10,000 using a sixth-order-accurate finite volume method for the discretization of convection and diffusion. The spatial discretization consists of a combination of a seventh-order upwind-biased method for the convective terms and an eighth-order central method for the diffusive terms, discretized on a stretched and staggered grid. To cope with the stretching of the grid, Lagrange interpolations are used.

The method applied to obtain a boundary condition for the velocity in the x-direction at the outflow boundary is shown not to affect the flow in the interior of the computational domain in a way that is visible in various snapshots of the vorticity field. The variation in the velocity in the x-direction with time is itself found to be relatively small near the outflow boundary.

Several turbulence statistics have been gathered from a simulation of the flow developed during 77 dimensionless time units. Snapshots of the vorticity field of the developed flow show the presence of a vortex-street-like structure. Typical 2D turbulent behaviour, such as the appearance of monopolar, dipolar and tripolar vortices due to the amalgamation of vorticity in the wake and the $x^{-1/2}$ scaling of the velocity defect in the wake, has been obtained.

Int. J. Numer. Meth. Fluids, **25**: 51–62 (1997).

No. of Figures: 9. No. of Tables: 0. No. of References: 11.

KEY WORDS: two-dimensional turbulence; DNS; vortex dynamics

1. INTRODUCTION

Two-dimensional flow around bluff obstacles is interesting because the results obtained in studying vortex-shedding phenomena are applicable to the construction of buildings (large rectangular boxes), cars, etc. Much work has been done in simulating 2D flow around such bluff obstacles at moderate Reynolds numbers. In particular, 2D flow around circular cylinders has been studied extensively. The transition process in the wake of a circular cylinder can only be described by two-dimensional numerical simulations such as performed by Gresho *et al.*,[1] Karniadakis *et al.*[2] and Braza *et al.*[3] for a small range of Reynolds numbers. Experiments report a strong three-dimensional behaviour when the Reynolds number exceeds 200.[4] A time trace of the streamwise velocity in the near wake of a circular cylinder in a two-dimensional simulation performed by Karniadakis and Triantafyllou[5] at $Re = 500$, however, shows that a time-periodic flow state is obtained, leading to the idea that the transition is caused entirely by three-dimensionality. The main difference between flow around a circular cylinder and flow around a square cylinder is the fact that only in the case of a square cylinder is the position of the frontal separation points fixed, which is found to have some influence on the dynamical behaviour of the flow in the transitional regime.[6] In this paper the 2D turbulent regime at $Re = 10{,}000$

Correspondence to: J. G. Wissink, Department of Theoretical Mechanics, University of Nottingham, University Park, Nottingham NG7 2RD, U.K.

CCC 0271–2091/97/010051–12 $17.50 *Received March 1996*

will be studied. Though 2D turbulence is quite different from its 3D counterpart, it is worth studying on its own merits. In geophysics and astrophysics, 2D turbulence is not an unusual phenomenon.[7] It is interesting to study which low-Reynolds-number structures persist in 2D turbulence. In 3D flow around a square cylinder, for instance, the 2D vortex street is still recognizable for Reynolds numbers larger than the Reynolds number at which the first 3D effects occur.[6] Another interesting feature of this 2D turbulent flow is the self-organization principle, which causes the emergence of some typical vortical structures (monopolar, dipolar and even tripolar) in the wake of the cylinder.

Having performed direct numerical simulations of various 1D and 2D test problems,[8] the seventh-order upwind-biased method and the fourth-order central method are found to be the most efficient methods for the discretization of the convection. The 2D flow simulation is more complex, because an outer flow has to be simulated. The main difficulty encountered is the treatment of the boundary condition downstream. This boundary condition needs to be prescribed such that it does not have a significant influence on the flow in the inner region of the domain. Attempting to use the fourth-order central method for the discretization of the convective terms led to spurious oscillations at the outflow boundary, causing the numerical scheme to become unstable. The seventh-order upwind-biased method, however, manages to suppress these non-physical oscillations such that the influence on the flow in the inner region is negligible.

The numerical method employed here is based on the marker-and-cell method of Harlow and Welch,[9] using a second-order-accurate central discretization of the conservation of mass and of the pressure gradient, combined in the interior of the computational domain with a seventh-order-accurate upwind-biased discretization of the first-order derivative in the convection and a sixth-order interpolation to cope with the staggering of the grid. The diffusive terms are discretized using an eighth-order-accurate central method.

Performing a simulation at $Re = 10{,}000$ using only 200×200 grid points resulted in spurious oscillations appearing near the corners of the cylinder. Upon enhancing the number of grid points to 400×400 (the number of grid points at which the actual simulations presented in this paper are obtained), these oscillations were found to disappear completely.

In Section 2 the test problem and the numerical method used to solve this problem are introduced. The numerical results approximating the flow in the turbulent regime are presented in Section 3, while in Section 4 a summary is given of the results obtained.

2. DESCRIPTION OF NUMERICAL EXPERIMENTS

In this paper, two-dimensional flow around a square cylinder at various Reynolds numbers is simulated. The Newtonian fluid in question is described by the incompressible Navier–Stokes equations, which consist of the following conservation laws: conservation of mass,

$$\nabla \cdot \vec{u} = 0, \tag{1}$$

and conservation of momentum (with the convection in non-conservative form),

$$\frac{\partial u}{\partial t} + u\frac{\partial u}{\partial x} + v\frac{\partial u}{\partial y} = -\frac{\partial p}{\partial x} + \frac{1}{Re}\nabla^2 u, \tag{2}$$

$$\frac{\partial v}{\partial t} + u\frac{\partial v}{\partial x} + v\frac{\partial v}{\partial y} = -\frac{\partial p}{\partial y} + \frac{1}{Re}\nabla^2 v, \tag{3}$$

where u is the velocity in the x-direction, v is the velocity in the y-direction and $Re = U_0 h/v$ is the Reynolds number (based on the height of the block, h, the characteristic velocity of the inflow field, U_0 and the kinematic viscosity v). Discretizing the Navier–Stokes equations using the

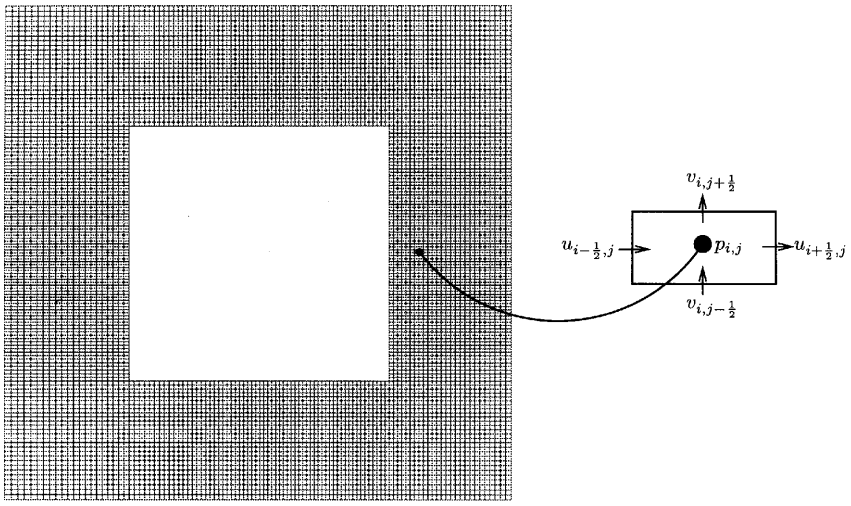

Figure 1. Stretched and staggered grid in neighbourhood of cylinder

primitive variables makes it straightforward to generalize the numerical discretization to 3D. The discretizations of the 2D Navier–Stokes equations are performed on a staggered grid as illustrated in Figure 1.

For some background material on the basic numerical algorithm we refer to Reference 9.

2.1. *Configuration of flow problem*

In Figure 2 the test problem is illustrated. The simulation is performed on several stretched grids. The cylinder is placed on the length axis ($y = 0$) of the computational domain. At the left-hand-side boundary (the inflow) the flow is prescribed to be uniform: the same boundary conditions are applied to the upper boundary and the lower boundary. To obtain a boundary condition for the x-velocity at the outflow boundary is more difficult. Because the Reynolds number of the flow is rather large, the diffusion term $\partial^2 u/\partial x$ at the right-hand-side boundary is neglected, parabolizing (2). The pressure gradient in the x-direction, $\partial p/\partial x$ (which is much smaller in the far wake than near the cylinder), is also neglected in order to obtain the equation

$$\frac{\partial u}{\partial t} = -u\frac{\partial u}{\partial x} - v\frac{\partial u}{\partial y} + \frac{1}{Re}\frac{\partial^2 u}{\partial y^2},$$

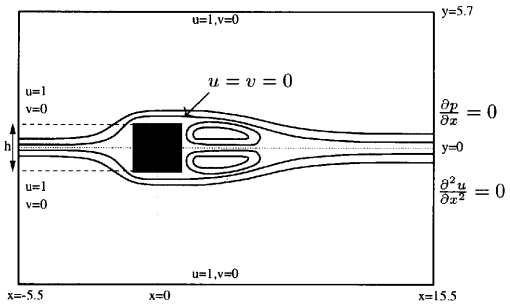

Figure 2. Configuration of flow problem

with which, using the second-order upwind scheme (20) to discretize $\partial u/\partial x$, the velocity u at the new time level $t = t_{n+1}$ at the outflow boundary is obtained.

The stretched grid in the x-direction is obtained by the transformation

$$(\delta x)_i = f_x h_x\{1 + \alpha \cos[(10\pi/6)(i - \tfrac{1}{2})h_x + \pi/3]\}, \tag{4}$$

where f_x is the multiplication factor needed to ensure that $\sum_{i=ibl}^{ibh-1} (\delta x)_i = 1$, h_x^{-1} is the number of grid points in the x-direction and α is a stretching parameter with a typical value of about $\frac{7}{10}$. In a similar way the stretched grid in the y-direction is defined by

$$(\delta y)_j = f_y h_y\{1 + \alpha \cos[2\pi(j - \tfrac{1}{2})h_y]\}, \tag{5}$$

where f_y is determined such that $\sum_{j=jbl}^{jbh-1} (\delta y)_j = 1$ and h_y^{-1} is the number of grid points in the y-direction. The parameters *ibl*, *ibh*, *jbl* and *jbh* determine the position of the cylinder in the grid.

2.2. Spatial discretization

In this subsection the numerical methods used for the discretization in space are described. For simplicity we assume the grid spacing to be equidistant and the grid width in the x-direction, δx, to be equal to the grid width in the y-direction, δy ($\delta x = \delta y = h$). Generalization to the stretched grid used in the numerical simulations is straightforward using Lagrange interpolations.

2.2.1. Discretization of conservation laws. Numerically the conservation of mass is described by

$$(\mathrm{div}_h^{(q)} \vec{u})^{n+1} = 0, \tag{6}$$

where q denotes the order of the central discretization used. The discrete form of the conservation of momentum can be written as

$$\frac{\vec{u}^{n+1} - \vec{u}^n}{\Delta t} = -(\mathrm{grad}_h^{(r)} p)^{n+1/2} + \begin{pmatrix} a^{n+1/2} \\ b^{n+1/2} \end{pmatrix}, \tag{7}$$

where the last vector on the right-hand side is a discretized form of the convective and diffusive terms and r denotes the order of the central FD method used; for example, putting $r = 2$ results in

$$\begin{aligned} \frac{u_{i+1/2,j}^{n+1} - u_{i+1/2,j}^n}{\Delta t} &= -\frac{p_{i+1,j}^n + 1/2 - p_{i,j}^{n+1/2}}{h} + a_{i+1/2,j}^{n+1/2}, \\ \frac{v_{i,j+1/2}^{n+1} - v_{i,j+1/2}^n}{\Delta t} &= -\frac{p_{i,j+1}^{n+1/2} - p_{i,j}^{n+1/2}}{h} + b_{i,j+1/2}^{n+1/2} \end{aligned} \tag{8}$$

Because we use a staggered grid, $(\mathrm{grad}_h^{(r)} p)_{i,j}^{n+1/2}$ must be evaluated at $(x_{i+1/2}, y_j)$ for the x-component and at $(x_i, y_{j+1/2})$ for the y-component. If we write (using the second-order-accurate explicit Adams–Bashforth scheme to obtain $\vec{a}$ at $t = t^{n+1/2}$)

$$\vec{a}^{n+1/2} = \begin{pmatrix} a^{n+1/2} \\ b^{n+1/2} \end{pmatrix} = \frac{3}{2}\begin{pmatrix} a^n \\ b^n \end{pmatrix} - \frac{1}{2}\begin{pmatrix} a^{n-1} \\ b^{n-1} \end{pmatrix},$$

the substitution of (7) into (6) results in the equation

$$\mathrm{div}_h^{(q)}(\mathrm{grad}_h^{(r)} p)_{i,j}^{n+1/2} = \frac{1}{\Delta t}(\mathrm{div}_h^{(q)} \vec{u})_{i,j}^n + (\mathrm{div}_h^{(q)} \vec{a})_{i,j}^{n+1/2}. \tag{9}$$

If we substitute $f_{i,j}^{n+1/2}$ for the right-hand side of (9), we obtain the standard form $\mathrm{div}_h^{(q)}(\mathrm{grad}_h^{(r)} p)_{i,j}^{n+1/2} = f_{i,j}^{n+1/2}$. Putting (for example) $q = r = 2$, we obtain the second-order-accurate discretization of (9) used in this study:

$$\frac{p_{i+1,j}^{n+1/2} + p_{i,j+1}^{n+1/2} - 4p_{i,j}^{n+1/2} + p_{i-1,j}^{n+1/2} + p_{i,j-1}^{n+1/2}}{h^2} = f_{i,j}^{n+1/2}. \tag{10}$$

2.2.2. Discretization of convective terms in non-conservative form. In (7) the discretized form of the convective and diffusive terms is referred to as a^n for the x-component of the momentum equation and b^n for the y-component. In this subsection we shall give these discretizations.

To get a discretization of the convective terms, we must obtain interpolated values $(I_{1,h}^{(m)}u)_{i,j}^n$ and $(I_{2,h}^{(m)}v)_{i,j}^n$ of u and v. In this notation, m is the order of interpolation. For example, taking $m = 2$ results in the discretization

$$\begin{pmatrix} (I_{1,h}^{(2)}u)_{i,j}^n \\ (I_{2,h}^{(2)}v)_{i,j}^n \end{pmatrix} = \begin{pmatrix} \frac{1}{2}(u_{i+1/2,j}^n + u_{i-1/2,j}^n) \\ \frac{1}{2}(v_{i,j+1/2}^n + v_{i,j-1/2}^n) \end{pmatrix}. \tag{11}$$

Central FD methods for the first-order derivative are dispersive in nature (i.e. their main truncation error is dispersive); this can lead to the occurrence of aliasing errors[10] which have to be controlled (e.g. by discretizing the convection in a kinetic-energy-conserving form) in order to be able to perform long-time integrations. Upwind and upwind-biased FD methods are dissipative in nature; because of this, more kinetic energy is dissipated at the smaller length scales than is the case when using central FD methods. That is the reason why upwind(-biased) discretizations of the convection do not need any other aliasing error control mechanisms and thus can be programmed in a non-conservative form. The corresponding discretization reads

$$\begin{aligned} (\mathrm{conv}_{x,h}^{(s,m)}\vec{u})_{i+1/2,j}^n &= u_{i+1/2,j}^n \frac{\partial}{\partial x}(u)_{i+1/2,j}^n + v_{i+1/2,j}^n \frac{\partial}{\partial y}(u)_{i+1/2,j}^n \\ &= u_{i+1/2,j}^n (B_{x,h}^{(s)}u)_{i+1/2,j}^n + (I_{2,h}^{(m)}(I_{1,h}^{(m)}v))_{i+1/2,j}^n (B_{y,h}^{(s)}u)_{i+1/2,j}^n \end{aligned} \tag{12}$$

for the convective term in the x-momentum equation and

$$\begin{aligned} (\mathrm{conv}_{y,h}^{(s,m)}\vec{u})_{i,j+1/2}^n &= v_{i,j+1/2}^n \frac{\partial}{\partial y}(v)_{i,j+1/2}^n + u_{i,j+1/2}^n \frac{\partial}{\partial x}(v)_{i,j+1/2}^n \\ &= v_{i,j+1/2}^n (B_{y,h}^{(s)}v)_{i,j+1/2}^n + (I_{1,h}^{(m)}(I_{2,h}^{(m)}u))_{i,j+1/2}^n (B_{x,h}^{(s)}v)_{i,j+1/2}^n \end{aligned} \tag{13}$$

for the convective term in the y-momentum equation. In both equations, s represents the order of the upwind-biased method. In the case where $u > 0$, the upwind-biased method $B_{x,h}^{(s)}u$ is defined for $s = 3$ by

$$(B_{x,h}^{(3)}u)_{i+1/2,j}^n = \frac{u_{i-3/2,j}^n - 6u_{i-1/2,j}^n + 3u_{i+1/2,j}^n + 2u_{i+3/2,j}^n}{6h}, \tag{14}$$

for $s = 5$ by

$$(B_{x,h}^{(5)}u)_{i+1/2,j}^n = \frac{-2u_{i-5/2,j}^n + 15u_{i-3/2,j}^n - 60u_{i-1/2,j}^n + 20u_{i+1/2,j}^n + 30u_{i+3/2,j}^n - 3u_{i+5/2,j}^n}{60h} \tag{15}$$

and finally for $s = 7$ by

$$(B^{(7)}_{x,h}u)^n_{i+1/2,j} = \frac{3u^n_{i-7/2,j} - 28u^n_{i-5/2,j} + 126u^n_{i-3/2,j} - 420u^n_{i-1/2,j} + 105u^n_{i+1/2,j} + 252u^n_{i+3/2,j} - 42u^n_{i+5/2,j} + 4u^n_{i+7/2,j}}{420h}. \tag{16}$$

2.2.3. Discretization of diffusive terms. The diffusive terms in the x-momentum equation are discretized as

$$(\mathrm{diff}^{(r)}_{x,h}u)^n_{i+1/2,j} = \frac{(D2^{(r)}_{x,h}u)^n_{i+1/2,j} + (D2^{(r)}_{y,h}u)^n_{i+1/2,j}}{Re}, \tag{17}$$

where r denotes the local order of accuracy; for example, for $r = 2$, $D2_{x,h}$ is defined by

$$(D2^{(2)}_{x,h}u)^n_{i+1/2,j} = \frac{u^n_{i+3/2,j} - 2u^n_{i+1/2,j} + u^n_{i-1/2,j}}{h^2}. \tag{18}$$

To get a discretization of a^n and b^n, we combine equation (12) with (17) and equation (13) with the discretization of the diffusion in the y-momentum equation and obtain

$$\begin{pmatrix} a^n \\ b^n \end{pmatrix} = \begin{pmatrix} -(\mathrm{conv}^{(s,m)}_{x,h}\vec{u})^n_{i+1/2,j} + (\mathrm{diff}^{(r)}_{x,h}u)^n_{i+1/2,j} \\ -(\mathrm{conv}^{(s,m)}_{y,h}\vec{u})^n_{i,j+1/2} + (\mathrm{diff}^{(r)}_{y,h}v)^n_{i,j+1/2} \end{pmatrix}. \tag{19}$$

2.2.4. Discretization at boundaries. In the neighbourhood of all boundaries, smooth transitions from the higher-order methods used in the interior of the computational domain to second-order methods are made. Such a smooth transition is made possible by selecting the intermediate discretizations such that they are of the same type as the discretization used in the inner region, except in the neighbourhood of the wall, where, when the flow is directed away from the wall, for the discretization of the first-order derivative in the convection the third-order upwind-biased method is replaced by the second-order central method instead of the first-order upwind method. This is illustrated in Figure 3, where full circles correspond to grid points where the discretized form of $u\partial u/\partial x$ is evaluated, open circles correspond to other nodes of the discretization stencil and $C^{(2)}_{x,h}$ is defined by

$$(C^{(2)}_{x,h}u)^n_{i+1/2,j} = \frac{u^n_{i+3/2,j} - u^n_{i-1/2,j}}{2h}.$$

Similarly, the eighth-order discretization of the diffusive terms in replaced by a sixth-, a fourth- and finally second-order method in the vicinity of the wall.

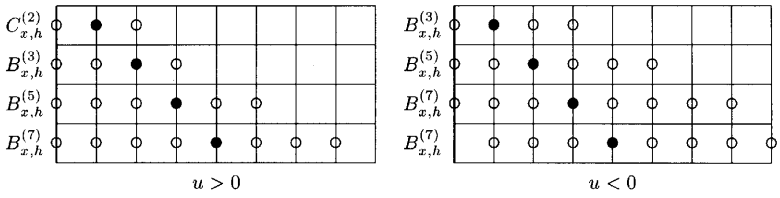

Figure 3. Discretization of $u\partial u/\partial x$ at left boundary

As mentioned before in Section 2.1, at the right-hand-side boundary the x-momentum equation is parabolized in order to obtain suitable boundary conditions for $u^{n+1}_{nx+1/2,j}$, $j = 1, \ldots, ny$. Using the second-order upwind discretization defined by

$$(B^{(2)}_{x,h}u)^n_{nx+1/2,j} = \frac{3u^n_{nx-3/2,j} - 4u^n_{nx-1/2,j} + u^n_{nx+1/2,j}}{2h}, \tag{20}$$

we obtain the convection term

$$(\mathrm{conv}^{(s,m)}_{\mathrm{rhs},x,h}\vec{u})^n_j = u^n_{nx+1/2,j}(B^{(2)}_{x,h}u)^n_{nx+1/2,j} + (I^{(m)}_{2,h}(I^{(m)}_{1,h}v))^n_{nx+1/2,j}(B^{(s)}_{y,h}u)^n_{nx+1/2,j}. \tag{21}$$

Using this, we are able to determine the boundary condition for u at $t = t_{n+1}$:

$$u^{n+1}_{nx+1/2,j} = u^n_{nx+1/2,j} + \Delta t\left(-(\mathrm{conv}^{(s,m)}_{\mathrm{rhs},x,h}\vec{u})^n_j + \frac{1}{Re}(D2^{(r)}_{y,h}u)^n_{nx+1/2,j}\right). \tag{22}$$

3. RESULTS

Using a 400 × 400 grid, a simulation at zero angle of attack has been performed at $Re = 10{,}000$. At the beginning of the simulation (starting with a uniform flow field), rather small vortices of opposite sign are shed in parallel, as illustrated by the perfect symmetry of the vorticity field plotted in Figure 4. The symmetric flow shown in this figure is, however, not a stable solution at $Re = 10{,}000$. Already at Re_{crit} somewhere between $Re = 45$ and 50 a Hopf bifurcation occurs.[6] The symmetric solution obtained for $Re < 45$ eventually breaks for $Re > Re_{\mathrm{crit}}$. Owing to small numerical errors, an unstable mode is introduced to the solution and eventually the symmetry of the solution will break.

After the breaking of the symmetry the flow behind the cylinder behaves very chaotically. A lot of very small vortices and filaments appear just behind the cylinder. Further away from the cylinder these small vortices amalgamate to form larger vortical structures. Several of these structures, such as monopolar, dipolar and even tripolar vortices, can be found in the snapshots plotted in Figure 5. Though the flow is turbulent (in the sense that it behaves chaotically), a vortex-street-like structure is still clearly visible at the back of the cylinder. This phenomenon is not unique. Snapshots of the

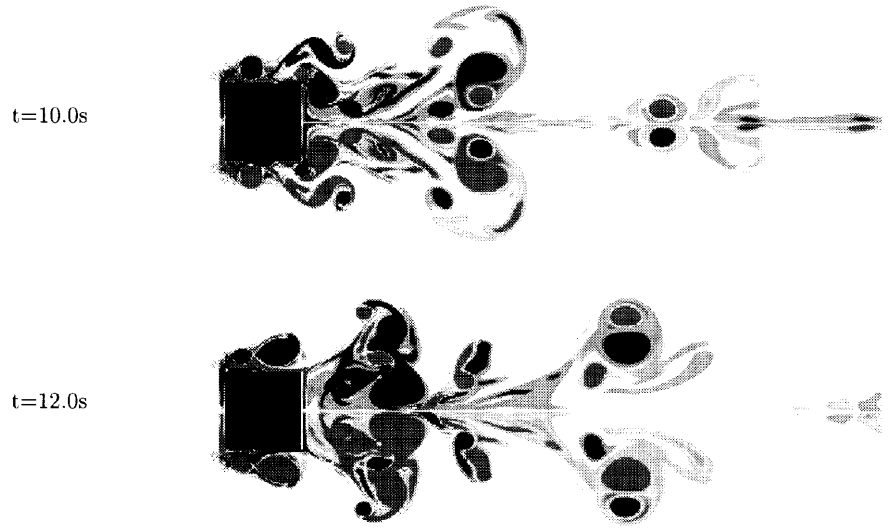

Figure 4. Two snapshots showing initial evolution of vorticity field at $Re = 10{,}000$ starting with uniform velocity field. Vortices of opposite sign are shed in parallel

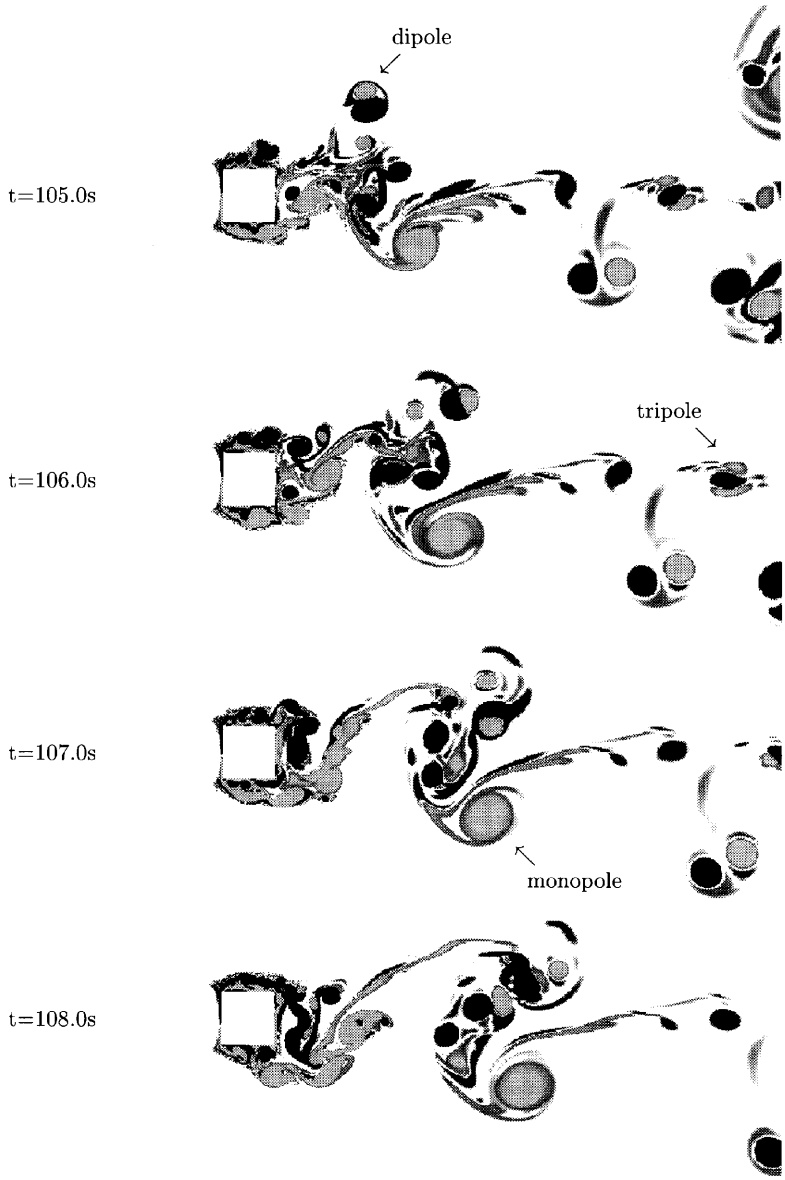

Figure 5. Four snapshots, each 1 s apart, showing evolution of vorticity field at $Re = 10{,}000$ a long time after breaking of symmetry. The light grey areas correspond to positive vorticity while the darker areas correspond to negative vorticity. The initially small vortical structures in the near wake of the cylinder amalgamate to form various kinds of coherent vortical structures further away from the cylinder

vorticity field at later times all show such a vortex-street-like structure. Thus we may conclude that it is not a transient phenomenon.

For 77 s* (corresponding to about 12 cycles of vortex shedding) a simulation of the developed turbulent flow at $Re = 10{,}000$ has been performed to gather some turbulence statistics. In Figure 6,

* In this paper the dimensionless time unit h/U_0 is referred to as 1 s.

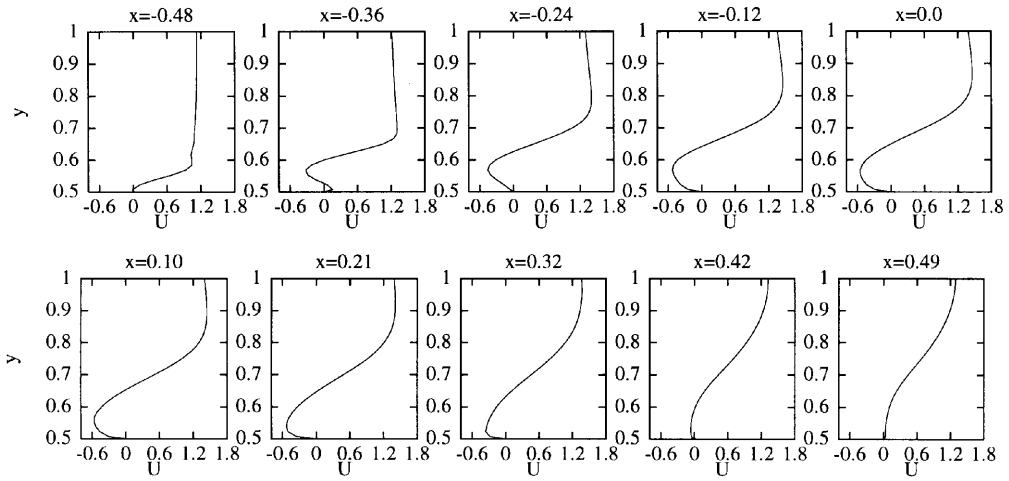

Figure 6. Mean u-velocity profiles at various stations along upper side of cylinder at $Re = 10{,}000$

time-averaged u-velocity profiles at the upper side of the cylinder are plotted. A large recirculation region covering almost the entire upper side of the block is clearly visible. Also, at $x = -0{\cdot}36$ (just behind the front corner of the cylinder) a small secondary recirculation region is visible.

The time-averaged (mean) u-velocity profiles plotted in Figure 7 have been gathered at various stations at which $x =$ constant behind the cylinder, each one unit length apart. The figure clearly illustrates the influence of the bluff body present upstream on the mean flow which is uniform at the left-hand-side boundary.

If $U_{\max}(x) = \max_y \bar{u}(x, y)$ and $U_{\min}(x) = \min_y \bar{u}(x, y)$ (where the bar denotes taking the mean value), then the mean velocity defect U_s is defined by

$$U_s(x) = (U_{\max} - U_{\min})(x).$$

Theoretically the mean velocity defect should obey the scaling law

$$U_s(x) \propto (x - x_0)^{-1/2}$$

in the far 2D turbulent wake for some fixed x_0.[11] Despite the fact that the turbulence statistics are gathered rather close behind the cylinder, the numerical results are found to obey this scaling law

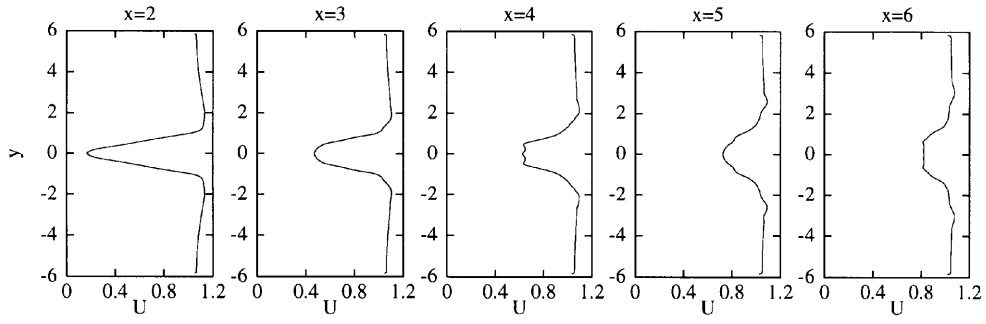

Figure 7. Mean u-velocity profiles at various stations through turbulent wake of cylinder at $Re = 10{,}000$

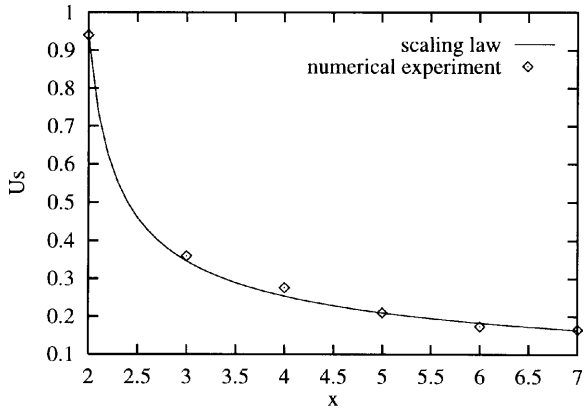

Figure 8. Comparison of numerical approximations of U_s at various stations through turbulent wake of cylinder with fitted graph of $U_{s,th}$ corresponding to theoretical scaling law

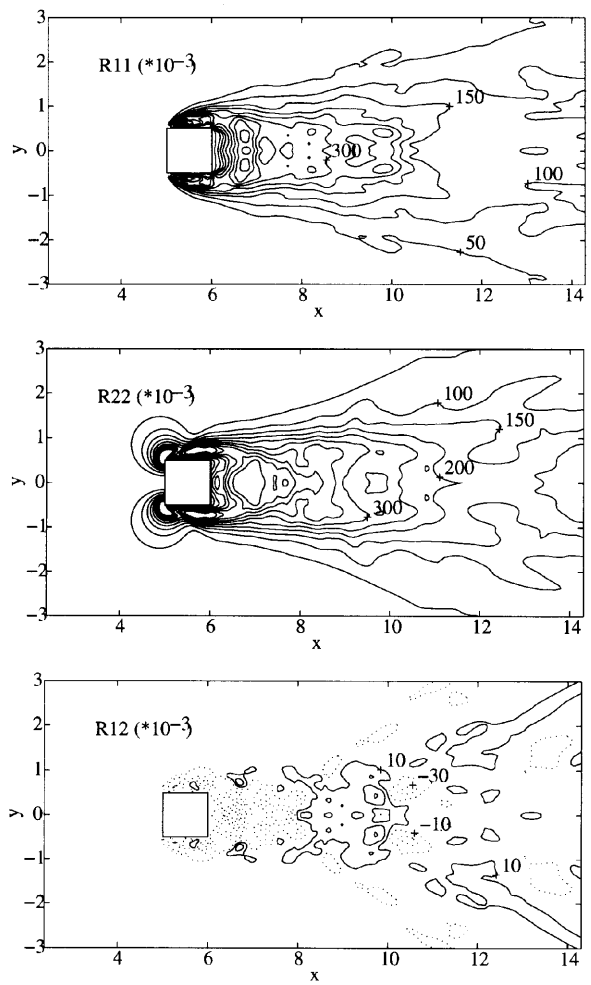

Figure 9. Reynolds stresses of turbulent flow around square cylinder at $Re = 10{,}000$ obtained during 77 s simulation of developed flow

very well. This is illustrated in Figure 8, where with the function $U_{s,th}(x) = 0{\cdot}373/\sqrt{(x - 1{\cdot}84)}$ a good fit of the numerical results is obtained.

If we denote the mean velocities by $U = \bar{u}$ and $V = \bar{v}$, then the fluctuating velocities are defined by $u' = U - u$ and $v' = V - v$. The Reynolds stresses $R11 = \overline{u'u'}$, $R12 = \overline{u'v'}$ and $R22 = \overline{v'v'}$ plotted in Figure 9 show that the part of the flow that is turbulent is spatially confined to rather small regions behind the cylinder and at the upper and lower sides of the cylinder. In the far wake the turbulence is found to decay.

Studying the snapshots presented in Figures 4 and 5 shows that the outflow boundary condition applied has no noticeable affect on the vorticity field in the interior of the computational domain. The only visible affect that occurred was some smearing of vorticity at the outflow boundary itself. Furthermore, the top graph in Figure 9 shows that in the neighbourhood of the outflow boundary the variation in u with time is relatively small, indicating that the omission of the pressure gradient in the parabolized x-momentum equation is justifiable.

4. CONCLUSIONS

Turbulent two-dimensional flow around a rectangular cylinder has been simulated. The simulations have been performed using a seventh-order upwind-biased method to discretize the convective terms (combined with a sixth-order interpolation to cope with the staggering of the grid) and an eighth-order central discretization for the diffusive terms. The results obtained at $Re = 10{,}000$ lead to the following conclusions.

1. Though the flow is turbulent, a vortex-street-like structure is still visible.
2. Owing to the amalgamation of vortices, various kinds of rather large vortical structures, such as monopolar, dipolar and tripolar vortices, appear in the wake of the cylinder.
3. At the upper and lower sides of the cylinder, (turbulent) shear layers develop accompanied by large recirculation regions just above and below the cylinder.
4. In the time-averaged velocity field, small secondary recirculation regions are present just behind the forward corners of the cylinder.
5. The mean velocity defect U_s in a large part of the turbulent wake of the cylinder is found to obey the scaling law $U_s \propto (x - x_0)^{-1/2}$ for some fixed number x_0.
6. The turbulence is found to be confined to rather small areas behind and at the upper and lower sides of the cylinder.

REFERENCES

1. P. M. Gresho, R. Chan, C. Upson and R. Lee, 'A modified finite-element method for solving the time-dependent, incompressible Navier–Stokes equations, Part 2. Applications', *Int. j. numer. methods fluids*, **4**, 619–640 (1984).
2. G. E. Karniadakis, E. T. Bullister and A. T. Patera, 'A spectral element method for solution of two- and three-dimensional time-dependent Navier–Stokes', *Proc. Eur.–U.S. Conf. on Finite-Element Methods for Nonlinear Problems*, Springer, Berlin, 1985, pp. 803–817.
3. M. Braza, P. Chassaing and H. Ha Minh, 'Numerical study and physical analysis of the pressure and velocity fields in the near wake of a circular cylinder', *J. Fluid Mech.*, **165**, 79–130 (1986).
4. C. H. K. Williamson, 'The existence of two stages in the transition to three-dimensionality of a cylinder wake', *Phys. Fluids*, **31**, 3165–3168 (1988).
5. G. E. Karniadakis and G. S. Triantafyllou, 'Three-dimensional dynamics and transition to turbulence in the wake of bluff objects', *J. Fluid Mech.*, **238**, 1–30 (1992).
6. J. G. Wissink, 'DNS of transitional flow around a square cylinder', in *Advances in Turbulence V*, Kluwer, Dordrecht, 1995, pp. 569–573
7. G. D. Earle and M. C. Kelley, 'Spectral evidence for stirring scales and two-dimensional turbulence in the auroral ionosphere', *J. Geophys. Res.*, **98**, 11,543–11,548 (1993).

8. J. G. Wissink, 'Direct numerical simulation of turbulence', Thesis, Rijksuniversiteit Groningen, 1995.
9. F. H. Harlow and J. E. Welch, 'Numerical calculation of time-dependent viscous incompressible flow of fluid with free surface', *Phys. Fluids*, **3**, 2182 (1965).
10. N. A. Phillips, 'An example of non-linear computational instability', in *The Rossby Memorial Volume*, Rockefeller Institute, New York, 1959.
11. H. Tennekes and J. L. Lumley, *A First Course in Turbulence*, MIT Press, Cambridge, MA, 1972.

